Available online at www.sciencedirect.com
ScienceDirect
Remote Sensing of Environment 108 (2007) 369–384
Remote Sensing of Environment
www.elsevier.com/locate/rse

# An intercomparison of the Surface Energy Balance Algorithm for Land (SEBAL) and the Two-Source Energy Balance (TSEB) modeling schemes

Wim J. Timmermans [a,*], William P. Kustas [b], Martha C. Anderson [b], Andrew N. French [c]

[a] Int. Inst. for Geo-Information Science and Earth Observation, P.O. Box 6, 7500 AA Enschede, The Netherlands
[b] USDA-ARS Hydrology and Remote Sensing Lab., Beltsville, MD 20705-2350 USA
[c] USDA-ARS U.S. Arid Land Agric. Res. Center, Maricopa, AZ 85239 USA

Received 1 March 2006; received in revised form 21 November 2006; accepted 24 November 2006

**Abstract**

An intercomparison of output from two models estimating spatially distributed surface energy fluxes from remotely sensed imagery is conducted. A major difference between the two models is whether the soil and vegetation components of the scene are treated separately (Two-Source Energy Balance; TSEB approach) or as a lumped composite (one-source approach; Surface Energy Balance Algorithm for Land; SEBAL) in the parameterization of radiative and turbulent exchanges with the overlying air. Comparisons are performed using data from two largescale field experiments covering sub-humid grassland (Southern Great Plains '97) and semi-arid rangeland (Monsoon '90) having very different landscape properties. In general, there was reasonable agreement between flux output from both models versus a handful of flux tower observations. However, spatial intercomparisons of model output over the full modeling domains yielded relatively large discrepancies (on the order of 100 W $m^{-2}$) in sensible heat flux ($H$) that are related to land cover. In particular, bare soil and sparsely vegetated areas yielded the largest discrepancies, with TSEB fluxes being in better agreement with tower observations. Modifications to SEBAL inputs that reduced discrepancies with TSEB and observations for bare soil and shrub classes tended to increase differences for other land cover classes. In particular, improvements to SEBAL inputs of surface roughness for momentum tended to exacerbate errors with respect to observed fluxes. These results suggest that some of the simplifying assumptions in SEBAL may not be strictly applicable over the wide range in conditions present within these landscapes. An analysis of TSEB and SEBAL sensitivity to uncertainties in primary inputs indicated that errors in surface temperature or surface-air temperature differences had the greatest impact on $H$ estimates. Inputs of secondary importance were fractional vegetation cover for TSEB, while for SEBAL, the selection of pixels representing wet and dry moisture end-member conditions significantly influenced flux predictions. The models were also run using input fields derived from both local and remote data sources, to test performance under conditions of varying ancillary data availability. In this case, both models performed similarly under both constraints.


*Keywords:* Remote sensing flux model; Single-source; Dual source; Land–atmosphere-interaction

## 1. Introduction

The partitioning of available energy between sensible and latent heat flux has a strong impact on atmospheric boundary layer development, which ultimately affects local and regional climate (Avissar & Pielke, 1989). Remotely sensed estimates of surface temperature derived from thermal satellite imagery convey valuable information regarding spatial variations in flux partitioning, and provide a means for remotely monitoring vegetation conditions and ecosystem health over the land surface (Moran, 2004).

Model parameterizations of the interaction between a land surface and the atmosphere are commonly called soil–vegetation–atmosphere transfer (SVAT) schemes. Numerous SVAT schemes have been developed in recent years with varying degrees of complexity, and with many designed to use remotely sensed surface temperature to estimate surface flux partitioning (Kustas & Norman, 1996). For homogeneous vegetation cover conditions, a single-source approach may be suitable, but in

* Corresponding author.
*E-mail address:* timmermans@itc.nl (W.J. Timmermans).

0034-4257/$ - see front matter © 2007 Elsevier Inc. All rights reserved.
doi:10.1016/j.rse.2006.11.028

most cases the landscape is under partial vegetation canopy cover so that both soil and vegetation components contribute to the net flux exchange as well as the remotely sensed signals (Norman et al., 1995). For more complex canopies, two-source modeling schemes provide a more realistic representation of the turbulent and radiation exchanges with the lower atmosphere (Huntingford et al., 2000; Lhomme et al., 1994; Merlin & Chehbouni, 2004; Norman et al., 2000; Shuttleworth & Wallace, 1985; Verhoef et al., 1997; Zhan et al., 1996).

In principle, two-source models have two sets of resistances across which individual, or local, source parameterization is applied and possibly a within-canopy air layer where such resistances meet, to allow interaction between the soil and vegetation component. A single aerodynamic resistance then connects the combined soil–canopy system with the local atmosphere. A one-source model uses only one resistance and assumes that all the surfaces can be represented by one effective value of temperature and humidity (Huntingford et al., 2000).

Since a large portion of the earth's land surface is only partially vegetated (such as in cropland and areas with sparse vegetation), a two-source model should generally reflect the surface energy balance with greater accuracy than a single-source scheme, especially if the two sources show very different radiometric behavior and atmospheric coupling. Still, many authors have found that after appropriate tuning of the model parameters, single-source models describe the overall surface energy balance satisfactorily in spite of their simplification of reality (Bastiaanssen et al., 1998b; Kustas et al., 1996; Troufleau et al., 1997). A simple but correctly calibrated single-source model might well out-perform an ill-parameterized dual source model (Kustas, 1990). However, local calibration is not generally possible for operational applications, rendering many one-source approaches useless when applied to new landscapes unless vegetation structure, fractional cover and other factors are considered (Matsushima, 2005; Su et al., 2001).

Remote sensing-based energy balance models tend to be validated with a handful of tower-based flux observations (Bastiaanssen et al., 1998b; Mecikalski et al., 1999), or more regionally with aircraft (Kustas et al., 2001, 2006a,b; Song et al., 2000). Although these validation experiments demonstrate that these models yield accurate surface flux estimates at the measurement sites, the question remains whether they are performing well over the broader landscape. Moreover, it is difficult to assess how generally applicable the models are outside the range of conditions sampled. To address these questions and to evaluate the uncertainty among various remote sensing-based SVAT models, intercomparisons of flux maps under a wide range of environmental conditions need to be performed. An intercomparison of single and dual source models by French et al. (2005) showed that despite systematic agreement for all flux components, the models had significant sensitivities to input uncertainties. Agreement in the turbulent fluxes was difficult to assess due to differences in model parameterizations, thus indicating the need for a further, in-depth analysis of each model.

In this study, a comparison is made between tower-based flux measurements and estimates from models representing single- and two-source SVAT schemes. A spatial intercomparison between the models is also performed over a range of environmental conditions. The comparisons are conducted over field campaign sites in Arizona (semi-arid climate) and Oklahoma (sub-humid), in landscapes having very different length scales of heterogeneity and a full range in cover and surface moisture conditions.

The main objective of this study is to assess whether the physical simplifications made in a one-source modeling scheme lead to significant errors in flux estimates, in comparison with the more detailed two-source modeling framework. In addition, a sensitivity analysis is performed to determine the inputs that cause significant uncertainty in model heat flux computations. The two models are also evaluated using both locally and remotely derived model input and calibrations, providing greater insight as to the utility of both modeling approaches when applied under different input constraints.

## 2. Model description

### 2.1. Model similarities

The one-source Surface Energy Balance Algorithm for Land (SEBAL) modeling scheme developed by Bastiaanssen et al. (1998a) is used here in conjunction with the iterative flux profile method (Gieske, 2003), implemented for calculation efficiency. The Two-Source Energy Balance (TSEB) model is described in Norman et al. (1995), with more recent updates in Kustas and Norman (1999) and Kustas et al. (2004). Both schemes use remotely sensed surface temperature as a primary boundary condition for providing estimates of instantaneous fluxes of net radiation ($R_N$), soil ($G$), sensible ($H$) and latent heat (LE). Both SEBAL and TSEB have been validated under a range of environmental conditions (Anderson et al., 2007; Bastiaanssen et al., 2005; Crow & Kustas, 2005).

Both schemes provide estimates of instantaneous surface fluxes by solving the energy balance equation:

$$R_N = G + H + \mathrm{LE} \tag{1}$$

net radiation estimation is quite similar for both models (and even interchangeable without significantly changing model results, see Section 6.2), following:

$$\begin{aligned} R_N &= R_S^{\downarrow} + R_S^{\uparrow} + R_L^{\downarrow} + R_L^{\uparrow} \\ &= (1-\rho_0)\cdot R_S^{\downarrow} + \varepsilon_0 \cdot \varepsilon_a \cdot \sigma \cdot T_a^4 - \varepsilon_0 \cdot \sigma \cdot T_R^4 \end{aligned} \tag{2}$$

where $R$ is radiation, with subscripts N, S, and L referring to net, shortwave and longwave, and the superscripted arrows indicate incoming (downward) and outgoing (upward) flux directions. The Greek letters $\rho$, $\varepsilon$, and $\sigma$ represent albedo, emissivity and the Stefan–Boltzmann constant, respectively, $T$ is temperature and the subscripts $R$ and $a$ refer to radiative surface and atmospheric level. For soil heat flux, both algorithms estimate $G$ as a fraction of the net radiation. In TSEB, the soil heat flux is determined as a fraction of the net radiation just above the soil surface as determined by modeling the divergence of net

radiation within the canopy using a simplified two-stream radiative transfer approach (Campbell & Norman, 1998). SEBAL uses a semi-empirical approach to estimate net radiation extinction in the canopy as a function of NDVI, surface temperature and albedo.

The main difference between the models involves the estimation of sensible heat flux and turbulent exchange coefficients, primarily in how the land surface is treated: either as a single-source (SEBAL), or as a dual source where the radiative and convective exchange processes between soil and vegetative canopies and the atmosphere are explicitly parameterized (TSEB). Both of these topics — formulation for $H$ and model inputs — are discussed in the next section.

### 2.2. Model differences

Apart from conceptual differences between the one-source and two-source modeling schemes, there are several other differences in how the TSEB and SEBAL models parameterize surface–atmosphere exchanges. The TSEB model initially assumes that the vegetation is unstressed and transpiring at the potential rate, then uses the radiometric surface temperature to constrain the canopy and soil components of $H$, and finally computes soil evaporation as a residual to the energy balance equation. If the resulting soil evaporation rate is negative (unlikely around midday on a clear day, when thermal satellite data are available), this is taken as a signature of vegetation stress and the canopy transpiration component of LE is throttled back (see Kustas & Norman, 1999; Kustas et al., 2004). SEBAL, on the other hand, is built on the assumption that full hydrological contrast (i.e., wet and dry pixels) is present in the area over which the imagery is acquired, and that an empirical relationship between $T_R$ and the difference between surface temperature and above-canopy air temperature can be developed within the context of the scene by properly selecting hot and cold pixels representing the conditions LE=0 and $H$=0, respectively. SEBAL calculates latent heat (no discrimination between soil and canopy components) as a residual of the energy balance equation. Since LE is computed in part or in whole as a residual by both models, it can accumulate multiple modeling errors. Therefore, the focus in this intercomparison is to assess differences in model fields of $H$.

Although both schemes use physically-based temperature gradient/resistance approaches to model $H$, the methodologies for estimating the gradients and resistances are very different. In SEBAL, the selection of the so-called dry and wet pixels (the hot and cold end-members of surface temperature) essentially determines the partitioning of available energy between $H$ and LE at all other pixels in the scene and helps to define resistance values. In SEBAL, $H$ is computed via a single-source resistance scheme,

$$H = \frac{\rho_a \cdot C_p}{r_{ah}} \cdot \delta\ T_{asur} \tag{3}$$

where $r_{ah}$ is the bulk aerodynamic resistance to heat transport and $\delta T_{asur}$ represents the difference between the surface aerodynamic temperature for heat ($T_{z0h}$) and above-canopy air temperature ($T_a$):

$$T_{z0h} - T_a = \delta\ T_{asur} = \frac{H \cdot r_{ah}}{\rho_a \cdot C_p} \tag{4}$$

The value of $T_{z0h}$ is related to the radiometric surface temperature, $T_R$, adjusting for the difference in the roughness lengths for momentum ($z_{0m}$) and heat ($z_{0h}$), which enter in the calculation of $r_{ah}$. This difference in roughness length is often referred to as the $kB^{-1}$ parameter (= $\ln(z_{0m}/z_{0h})$) and is generally taken to be on the order of 2 for vegetation (Garratt & Hicks, 1973), but can be much larger for sparse canopies, with values of 12 derived over savannah (Verhoef et al., 1997). In SEBAL, a nominal $kB^{-1}$ value of 2.3 is applied over the entire scene, tying $z_{0h}$ to a fixed fraction (1/10) of $z_{0m}$. The roughness length for momentum must then be specified over the scene. In the original version of SEBAL (Bastiaanssen et al., 1998a) and more recent implementations (e.g., Jacob et al., 2002), $z_{0m}$ was estimated using an exponential relation with NDVI:

$$z_{0m} = \exp^{(c_1 + c_2 \cdot \mathrm{NDVI})} \tag{5}$$

where coefficients $c_1$ and $c_2$ are locally calibrated, if possible. Later studies recognized that in addition to NDVI, canopy height is also critical to determining surface roughness, necessitating additional information on land cover/land use (Tasumi et al., 2000).

In the SEBAL methodology, $\delta T_{asur}$ is not specified a priori using observed temperature gradients, but rather deduced from the surface radiometric temperature field under the assumption that $\delta T_{asur}$ is linearly related to $T_R$. Using an aggregation–disaggregation technique for assigning local scale friction velocity, an estimate of the aerodynamic resistance to heat, $r_{ah}$, is computed for each pixel using values of $z_{0h}$ and $z_{0m}$ specified as discussed above. Eq. (4) is then solved by flux inversion to evaluate $\delta T_{asur}$ at the hydrological extremes ($H$=0 and $H = R_N - G$) using representative cold and hot pixels within the scene. The values of $T_R$ and $\delta T_{asur}$ derived at these endpoint pixels are used to calibrate a linear relationship, assumed to be valid across the entire modeling domain:

$$\delta T_{asur} = a \cdot T_R - b \tag{6}$$

where $a$ and $b$ are linear regression coefficients that are site and scene specific (Bastiaanssen et al., 1998a). At all other pixels, $\delta T_{asur}$ is retrieved from $T_R$ using Eq. (6), and $H$ is computed from Eq. (4) given the pixel estimate of $r_{ah}$. It is assumed that deviations of actual $z_{0h}$ from the nominal value of $kB^{-1}$=2.3 are absorbed into the calibrated regression equation, thus reducing the need for accurate specification of $z_{0h}$ (and therefore $r_{ah}$) at each pixel. Implicit in the application of Eq. (6) is the assumption that $kB^{-1}$ is also linearly related to $T_R$ across the scene of interest, and is adequately constrained by flux inversion at the selected end-member pixels. This assumption is fundamental in the calculation of $H$ for SEBAL, (Jacob et al., 2002; Norman et al., 2006). Details on the procedure above can be found in Bastiaanssen et al. (1998a, 2002) and Su et al. (1999).

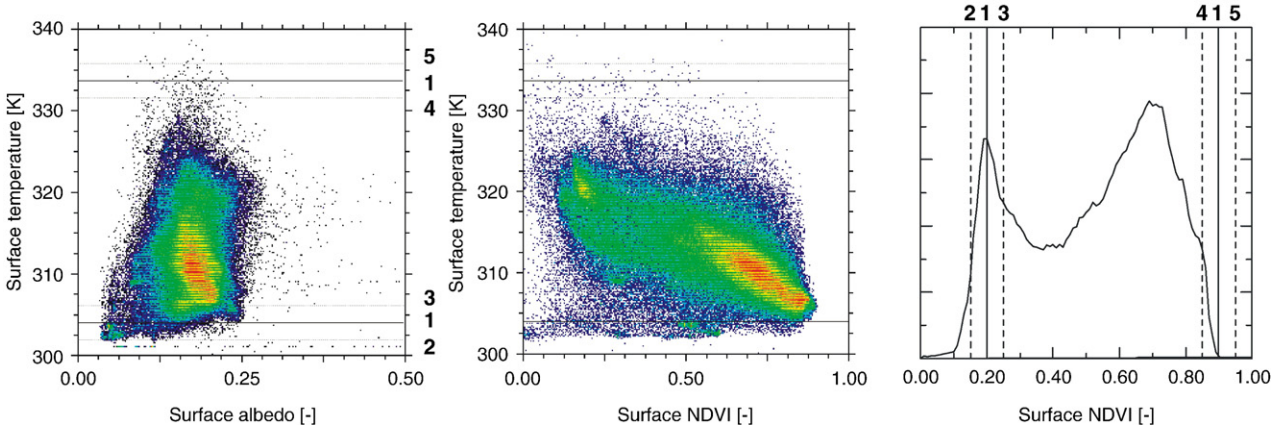


Fig. 1. Selecting minimum and maximum end-members of key inputs for the two schemes, example DOY 183 during the SGP '97 experiment. Two-dimensional scatterplots of surface temperature versus surface reflection and NDVI respectively to illustrate the selection of "wet" and "dry" surface temperature end-members in the SEBAL scheme, and the NDVI histogram to select the values between which to scale the NDVI in the TSEB scheme. Solid lines represent the actual values chosen (reference values), whereas the dotted lines represent values that are used to show the sensitivity of the model output to these parameters. The numbers refer to the different scenarios described in the main text (see also Table 1).

Following the original SEBAL formulation, the dry and wet end-members are to be determined from the image itself, using the observed $T_R - \rho_0$ and $T_R - \mathrm{NDVI}$ relations, as shown in the scatterplot in Fig. 1. This process can be difficult, since selection and re-selection as well as some subjective decision-making are required (Tasumi et al., 2000). However, similar approaches for deriving near surface air temperature from observed surface temperatures exist (Nemani & Running, 1989; Prihodko & Goward, 1997; Prince et al., 1998), where also $T_R - \mathrm{NDVI}$ scatterplots are used to facilitate determining the relevant end-members in Fig. 1.

The wet pixel is selected at a location that has the lowest surface temperature, but that is known to have vegetation cover. Open water bodies should in general be avoided, due to the problem of estimating the heat storage term, which is typically much larger than $G$ for land surfaces and has a more significant time lag. If such areas are not available in the scene, another option is to take the wet end-member equal to the near-surface or screen level air temperature from the nearest weather station. There is no consensus on how to select the hot pixel. Bastiaanssen (1995) originally proposed to use the 95 percentile hottest pixel in the image. However, this may create problems, since multiple pixels with different roughness values may fit this criterion and hence a subjective decision is still required in selecting the hot pixel. Tasumi et al. (2000) proposed using the hottest location in the image, preferably a man-made surface. Another option that has been proposed is to select the hot pixel having the lowest (relative) surface temperature, but that is known a priori to be completely dry (Bastiaanssen, 2002; personal communication).

For the TSEB model, an estimate of fractional vegetation cover, $f_c$ ($\phi$), apparent at view angle, $\phi$, is needed to partition the ensemble directional radiometric temperature, $T_R$ ($\phi$), into the temperatures for the soil and vegetation components via

$$T_R(\phi) \approx \left[ f_c(\phi) \cdot T_c^4 + (1 - f_c(\phi)) \cdot T_s^4 \right]^{1/4} \quad (7)$$

The vegetation and soil temperatures ($T_c$ and $T_s$, respectively) then help to define the partitioning of available energy between $H$ and LE. The sensible heat from the soil ($H_s$) and vegetated canopy ($H_c$) and composite system ($H$) was computed using the parallel resistance formulation originally developed in Norman et al. (1995), but with a slight modification to the canopy resistance formulation:

$$H_s = \rho_a \cdot C_P \frac{T_s - T_a}{r_s + r_a}$$

$$H_c = \rho_a \cdot C_P \frac{T_c - T_a}{r_{ah}}$$

$$H = H_c + H_s \quad (8)$$

where $r_s$ is the aerodynamic resistance to heat transfer from the soil, $r_a$ is the aerodynamic resistance from the canopy air layer above the soil (at height $z_{0m} + d_0$, where $d_0$ is the displacement height) to a reference level several meters above the canopy where $T_a$ (and wind speed) is measured, and $r_{ah}$ is similar to the $r_{ah}$ formulation for SEBAL, assuming $kB^{-1} = 2$. For details on the resistance formulations see Norman et al. (1995) and Kustas and Norman (1999). Typically in TSEB applications, the momentum roughness $z_{0m}$ is estimated as a fraction of the canopy height, $h_C$, namely $z_{0m} = 1/8\ h_C$ while the displacement height is $d_0 = 2/3\ h_C$, which is reasonable for vegetated canopies (Brutsaert, 1982). Norman et al. (1995) also give a series resistance formulation for the TSEB, where soil and canopy fluxes jointly modify the microclimate inside the canopy, generating feedback on the fluxes themselves. While the series model likely gives a more accurate micrometeorological description of the system, both versions of the TSEB were found to give similar results for a wide range in cover conditions (Li et al., 2005). The parallel version was implemented here for simplicity.

Table 1
Values for $S_i$ (%) for the two models with±25% variation in the model parameters from their reference values

| Model parameter | TSEB | | Model parameter | SEBAL | |
|---|---|---|---|---|---|
| | −25% $S_i$ (%) | +25% $S_i$ (%) | | −25% $S_i$ (%) | +25% $S_i$ (%) |
| $z_{0m}$ | 1. | −3 | $\rho_0$ | 16 | −10 |
| $T_R^1$ | −44 | 74 | $T_R^1$ | 17 | −9 |
| $T_a^1$ | 6 | −7 | $z_{0m}$ | −5 | −6 |
| $U$ | −7 | 7 | $kB^{-1}$ | 2 | 4 |
| $h_c$ | −1 | −0.5 | $\delta T_{asur}$ | −45 | −3 |
| $f_c$ | −19 | 46 | NDVI | −11 | 27 |
| LAI | −15 | 30 | | | |
| End-member | | | | | |
| $NDVI_{min}$ | 5 | −4 | $T_{R\text{-}min}$ | 20 | −24 |
| $NDVI_{max}$ | 24 | −9 | $T_{R\text{-}max}$ | 15 | −27 |

Note: A different variation is taken for temperature values (±1%)[1] due to unrealistic deviations when using±25%. For the upper and lower limits (end-members), a fixed deviation of ±0.05 (NDVI) and ±2 K ($T_R$) is taken from their reference values.

One method that has been used to retrieve $f_c$ (0) ($\phi$=0, nadir view angle) from remote sensing data is a scaled NDVI approach (Choudhury et al., 1994):

$$f_c(0) = 1 - \left(\frac{NDVI_{max} - NDVI}{NDVI_{max} - NDVI_{min}}\right)^p \quad (9)$$

where the end-member NDVI values, $NDVI_{max}$ and $NDVI_{min}$, represent a surface fully covered by vegetation and completely bare, respectively. The parameter $p$ represents the ratio of a leaf angle distribution term, $\Lambda$, ((=0.5 for spherical distributions; Ross, 1975) to canopy extinction, $\kappa$, where $p=\Lambda/\kappa$. As in SEBAL, the selection of NDVI end-members has some uncertainty, although with a NDVI histogram analysis, the selection of the minimum and maximum values can be fairly accurate (see Fig. 1). Leaf area index (LAI), used in the computation of net radiation divergence and wind speed decay through the canopy layer (Kustas & Norman, 1999), can be related to $f_c$ (0):

$$LAI = \frac{\ln(1 - f_c(0))}{\Lambda} \quad (10)$$

(Choudhury, 1987). Apparent cover fraction at view angle $\phi$ is then obtained with

$$f_c(\phi) = 1 - \exp\left(\frac{-\Lambda \cdot \Omega(\phi) \cdot LAI}{\cos\phi}\right) \quad (11)$$

where the directional clumping factor $\Omega(0)$ depends on canopy architecture, as specified in Kustas and Norman (1999). Note that the scaled NDVI approach to estimating $f_c$ and LAI is not an integral part of the TSEB — other techniques exist for estimating these surface parameters from remote sensing data, such as inversion of the bi-directional reflectance function.

The more detailed description of radiation and turbulent flux exchange in the TSEB model requires specification of several parameters relating to canopy architecture; namely canopy height, leaf width, and vegetation clumping factor — these are typically assigned by land cover class. However, sensitivity studies evaluating the uncertainty of the inputs to TSEB model flux computations indicated that nominal values for most of the canopy and roughness parameters can be used without causing significant error (Anderson et al., 1997; Kustas & Norman, 1999; Zhan et al., 1996). Furthermore, the data requirements are similar to one-source schemes that, unlike SEBAL, explicitly account for differences in aerodynamic and radiative temperatures (Matsushima, 2005). In situations where the local meteorological data (air temperature and wind speed) required by the TSEB are unavailable, a nested modeling approach can be used to supply these inputs (Anderson et al., 2004; Norman et al., 2003).

The SEBAL scheme derives necessary aerodynamic roughness and resistance directly from remote sensing data using semi-empirical relations. Moreover, SEBAL does not require local $T_a$ nor wind speed inputs, other than regional averages and some estimate of the blending height (Su et al., 1999).

## 3. Experimental data

Data from two experimental sites were used in the model intercomparisons, representing very different landcover conditions in terms of canopy structure and spatial distribution of

Table 2
Description of the statistics used in assessing the model performance

| Statistical variable | Description | Equation |
|---|---|---|
| $N$ | Number of observations | |
| $<O>$ | Mean of the observed variable | $\frac{1}{n}\sum_{i=1}^{n} O_i$ |
| $<P>$ | Mean of the model-predicted variable | $\frac{1}{n}\sum_{i=1}^{n} P_i$ |
| So | Standard deviation of the observed variable | $\left[\sum_{i=1}^{n} \frac{(O_i - <O>)^2}{n-1}\right]^{1/2}$ |
| Sp | Standard deviation of the model-predicted variable | $\left[\sum_{i=1}^{n} \frac{(P_i - <P>)^2}{n-1}\right]^{1/2}$ |
| MAD | Mean absolute difference | $\frac{1}{n}\sum_{i=1}^{n} \lvert P_i - O_i\rvert$ |
| MAPD | Mean absolute percent difference | $\frac{100}{<O>}\left(\frac{1}{n}\sum_{i=1}^{n} \lvert P_i - O_i\rvert\right)$ |
| RMSD | Root-mean-square difference | $\left[\frac{1}{n}\sum_{i=1}^{n} (P_i - O_i)^2\right]^{1/2}$ |

vegetation across the landscape. Both sites, however, have significant areas of sparse vegetation cover — challenging conditions for single-source modeling schemes.

The first dataset was collected during the Monsoon '90 field experiment (Kustas et al., 1994), conducted in a semiarid rangeland area within the USDA-ARS Walnut Gulch Experimental Watershed near Tucson, Arizona. This region is comprised primarily of shrubs ranging from nominally 25% canopy cover for upland areas and up to 75% cover along ephemeral channels, with a few areas still supporting primarily a grassland ecosystem having generally less than 40% cover. During the field campaign, aircraft-based visible (VIS), near-infrared (NIR) and thermal-infrared (TIR) images at nominally 6 m resolution were collected on 3 days representing dry (Day of Year—DOY 213), wet (DOY 216) and intermediate (DOY 221) soil moisture conditions (Humes et al., 1997; Schmugge et al., 1998). In addition, eight micrometeorological towers were distributed over the watershed, sampling fluxes and atmospheric conditions over representative land cover types (Kustas et al., 1994).

The second dataset was collected during the Southern Great Plains experiment of 1997 (SGP '97) near EL Reno, Oklahoma (Jackson et al., 1999). This region is primarily comprised of grass lands/pastures and large tracts of winter wheat crop, which by late June (start of the field campaign) was harvested wheat stubble or tilled bare soil. Remote sensing observations at VIS, NIR and TIR wavelengths were collected using the Thermal Infrared Multi-spectral Scanner (TIMS) and the Thematic Mapper Simulator (TMS) airborne instruments at nominally 12 m resolution (French et al., 2000, 2003b). Data from 2 days during late June and early July 1997, representing wet (DOY 180) and intermediate (DOY 183) surface moisture conditions, are used. This study also uses data collected at four flux towers operating in the El Reno study area, representing the main land cover types with LAI ranging from 0 to 4 (Twine et al., 2000).

In the TSEB, the canopy extinction factor $\kappa$ was set to 0.45 for the Monsoon site (Anderson et al. (1997) and 0.8 for the SGP site, (French et al., 2003b). The vegetation clumping factor $\Omega(0)$ is set to unity for both sites (no clumping). Although for the Monsoon site this clumping factor is likely to be less than one, the methods used to measure LAI implicitly included the clumping effect, and previous studies have demonstrated that a clumping factor of 1 gives reasonable results in this case (Anderson et al., 1997; Norman et al., 1995).

## 4. Model sensitivity

In order to directly compare model sensitivities and their dependencies on surface conditions, a sensitivity analysis for both models was performed using the dataset from SGP '97 on

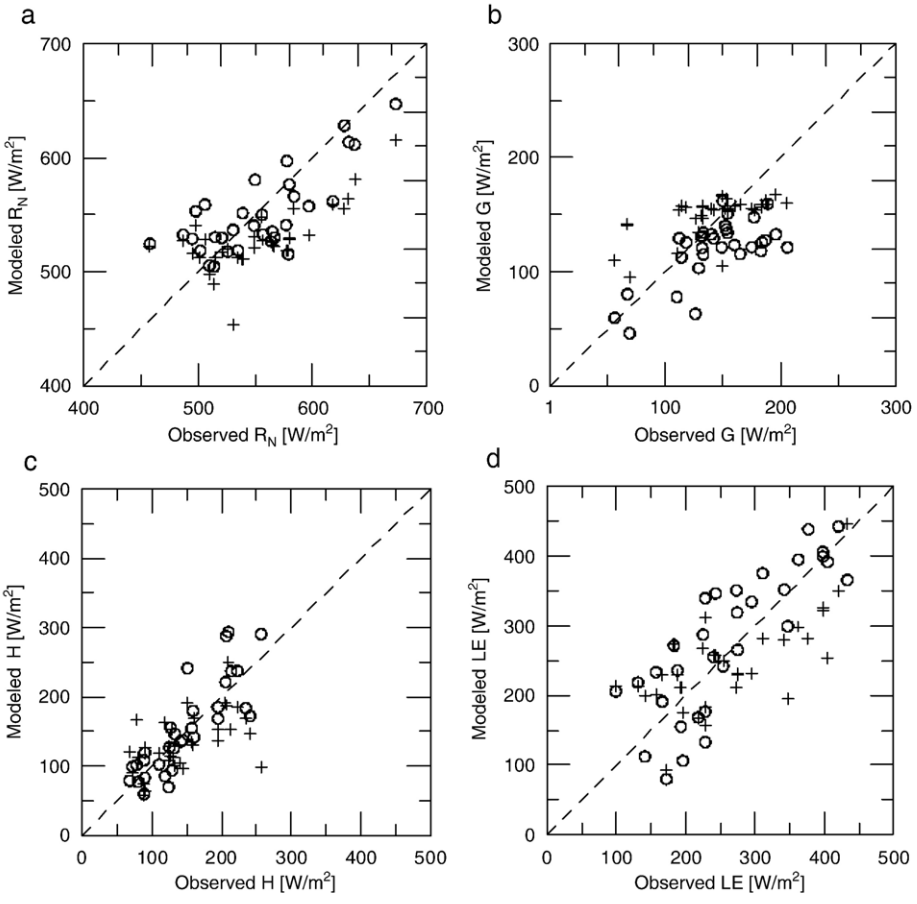


Fig. 2. Modeled versus observed energy balance components a) $R_N$, b) $G$, c) $H$, d) LE for the Monsoon '90 (DOY 213, 216 and 221) and SGP '97 (DOY 180 and 183) for both schemes. The cross symbols represent SEBAL and circles TSEB output.

Table 3
Statistics of model performance for computing surface energy balance components for both sites

| Component | Model | <O> | <P> | <So> | <Sp> | MAD | MAPD | RSMD |
|---|---|---|---|---|---|---|---|---|
| Rn | SEBAL | 554 | 528 | 49 | 28 | 38 | 7 | 44 |
| Rn | TSEB | 554 | 551 | 49 | 36 | 26 | 5 | 32 |
| *G* | SEBAL | 143 | 149 | 36 | 18 | 24 | 16 | 29 |
| *G* | TSEB | 143 | 120 | 36 | 27 | 27 | 19 | 35 |
| *H* | SEBAL | 148 | 135 | 55 | 42 | 39 | 26 | 49 |
| *H* | TSEB | 148 | 153 | 55 | 67 | 28 | 19 | 37 |
| LE | SEBAL | 262 | 245 | 93 | 66 | 61 | 23 | 70 |
| LE | TSEB | 262 | 278 | 93 | 103 | 53 | 20 | 62 |

DOY 183, representing a range of environmental and land cover characteristics. The model domain on this date exhibited patchy moisture conditions following a large precipitation event on DOY 179, while LAI varied from 0 in bare, harvested winter wheat fields to ~ 4 in dense grassland and riparian areas. Sensitivity tests were performed for input variables that most significantly affect $H$ computation in the TSEB and SEBAL algorithms (see Table 1), as summarized by Eqs. (3) and (8). Although $\delta T_{asur}$ is derived from Eq. (6), and hence not technically a direct input to SEBAL, it is still important to assess the impact of uncertainties in $\delta T_{asur}$ as retrieved from this simplified linear relationship with $T_R$. Simulations with a detailed soil–plant–atmosphere model indicate that Eq. (6) can yield large retrieval errors (>5 °C) in $\delta T_{asur}$ over scenes with widely varying roughness and vegetation stress conditions (Norman et al., 2006).

In this analysis the sensitivity $S_i$ of a model to an input $i$ is defined as:

$$S_i = \left(\frac{H_{\pm} - H_0}{H_0}\right) * 100 \quad (12)$$

where $H_0$, $H_+$ and $H_-$ are the sensible heat flux predicted by the model when the input equals its reference value $i_0$, $1.25 \cdot i_0$ and $0.75 \cdot i_0$, respectively, with reference values used for all other inputs. To capture a range in surface conditions, the sensitivity tests were performed over the full SGP '97 modeling domain. The reference input fields were obtained from local observations and calibrations, as described in Section 5.1, and $H_0$ was computed across the domain. The values at each pixel in the target input reference field were then perturbed to compute $H_+$ and $H_-$. Finally, $H_0$, $H_+$ and $H_-$ values for several pixels encompassing the 4 tower sites were then averaged. As such, these fluxes are assumed to be representative of the average vegetation cover and moisture conditions, and surface temperature states for this region, since the tower locations have been shown to be fairly representative of the observed local variability (Norman et al., 2003). The 25% deviation from $i_0$ was not applied to surface/air temperature (K) since such a departure exceeds the physical limits of these inputs (see Table 1). Instead, a 1% variation from $i_0$ in surface/air temperatures was used. Note that in the case of surface temperature this amounts to about 3° deviation, which is almost twice the uncertainty observed for atmospherically corrected surface temperatures under these circumstances (French et al., 2003a, 2000).

From the results in Table 1, it appears that variations in SEBAL estimates of $H$ are less than 20% for the prescribed 25% deviations in 4 out of the 6 input variables while for the TSEB, variations in $H$ estimates are less than 10% for 4 out of the 7 inputs. SEBAL is most sensitive to deviations in $\delta T_{asur}$, with $S_i$ reaching 45%, followed by sensitivity in NDVI ($S_i \sim 30\%$) and albedo ($S_i \sim 15\%$). The TSEB model has greatest sensitivity to the variation in $T_R$ yielding deviations from the reference $H$ value of up to 75%, followed by $f_c$ and LAI, with $S_i \sim 45\%$ and 30%, respectively. As shown in previous studies, the other inputs for the TSEB scheme, such as vegetation properties and roughness characteristics, do not contribute to significant errors in $H$ estimates (Anderson et al., 1997). Thus, both models have the greatest sensitivity to errors in remotely sensed surface temperature and surface–air temperature differences. Naturally, sensitivities for both models will depend to some extent on the

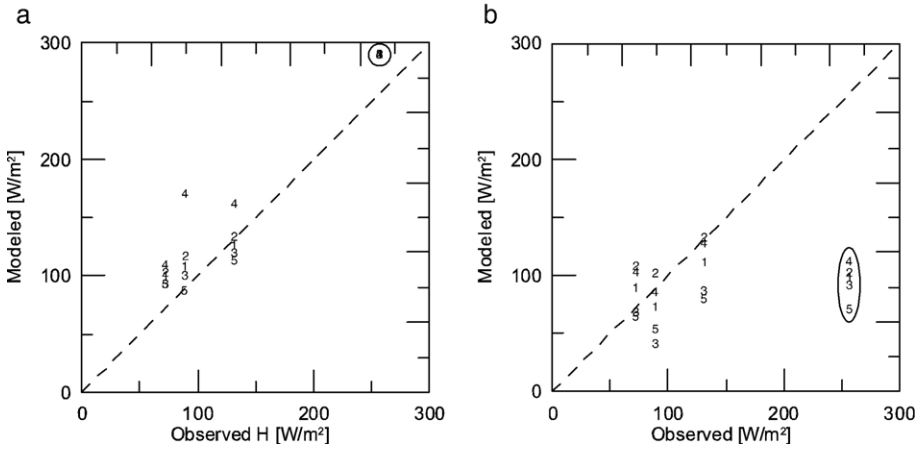


Fig. 3. Model sensitivity in sensible heat output for DOY 183 in SGP '97 to changes in NDVI end-members for a) TSEB and in surface temperature end-members for b) SEBAL. The numbers refer to the different scenarios described in the main text (see also Table 1): Scenario "1" represents the original parameter setting, a "2" means the minimum end-member is lowered, whereas a "3" indicates the minimum value is taken higher, a "4" means the maximum is lowered and a "5" represents a higher value for the maximum. Values from the bare soil site (ER13) are encircled.

exact choice of the reference values, but this type of detailed sensitivity analysis is beyond the scope of the present study. Here, area-average conditions are computed from the 4 flux tower locations to produce "average" sensitivities, which are confirmed by previous sensitivity studies (e.g., Anderson et al., 1997; Zhan et al., 1996).

The sensitivity of TSEB to uncertainty in surface temperature is greatly reduced when the TSEB is coupled with an atmospheric boundary layer (ABL) model, allowing the air temperature at the blending height (~50 m) to be derived internally within the model, adjusting to biases in $T_R$ (Anderson et al., 1997). Such a modeling framework has permitted the development of a robust and operational remote sensing-based approach for flux monitoring at regional scales (Anderson et al., 2003; Diak et al., 2004).

The sensitivity of both schemes to end-member selection in $T_R$ (SEBAL) and NDVI (TSEB) was also tested with the DOY 183 SGP '97 dataset. Reference end-member values of $T_R$ used in SEBAL in scenario 1 were $T_{R\text{-min}}$=304 K and $T_{R\text{-max}}$=333.7 K (average values computed from several representative pixels). The model was then re-run holding the dry end-member constant at the reference value and modifying the wet end-member by −2 K (scenario 2) and +2 K (scenario 3). Additional runs were performed thereafter by keeping the wet end-member at the original value, and selecting dry end-member pixels with temperatures −2 K (scenario 4) and +2 K (scenario 5) with respect to the reference temperature (see Fig. 1). A similar set of scenarios was generated for the TSEB (see also Fig. 1): varying the reference $NDVI_{min}$ (0.20) by −0.05 and +0.05 (scenarios 2 and 3, respectively), and varying the reference $NDVI_{max}$ (0.90) by −0.05 and +0.05 (scenarios 4 and 5, respectively).

Model sensitivities to changes in end-member values are presented at the bottom of Table 1. In general, uncertainty in the selection of either the upper or lower limits of $T_R$ in SEBAL tend to result in similar effects on the magnitude of variation in $H$ (on the order of 20–25%). The TSEB shows more sensitivity ($S_i$~25%) to variations in $NDVI_{max}$, defining full vegetation cover conditions. At high cover, it becomes more difficult to separate soil and canopy temperatures and fluxes and the TSEB is more sensitive to uncertainties in $T_R(\phi)$ (Anderson et al., 2005; Kustas et al., 2003).

## 5. Model validation

### 5.1. Validation strategy

In validating flux predictions from both modeling schemes with respect to observed fluxes, the original formulations of both models (as described in Section 2) were implemented and where applicable, local calibration was performed or local measurements of input data were used. For the SEBAL scheme, this meant adjusting the empirical coefficients, $c_1$, $c_2$ and $c_3$ in:

$$\Gamma = T_R/\rho_0 \cdot (c_1 \cdot \rho_0^{avg} + c_2 \cdot \rho_0^{avg^2}) \cdot (1 - c_3 \cdot NDVI^4) \quad (13)$$

where $\Gamma$ is the assumed ratio between soil heat flux and net radiation. In general practice, these adjustments are made using measurements of NDVI, surface temperature and instantaneous and daytime averaged (avg) surface albedo along with soil heat flux and net radiation measurements. Momentum roughness in SEBAL was estimated using the NDVI relationship in Eq. (5). The TSEB does not use any locally calibrated coefficients; however, in this exercise ground-based observations of canopy height were used to estimate roughness parameters for the major land cover types, which were then spatially distributed using a land cover image (French et al., 2003b; Schmugge et al., 1998). Meteorological data (primarily wind speed, air temperature, and solar radiation) used in both models were obtained locally from the flux tower networks within the modeling domains.

Validation of model output was performed in comparison with tower-based flux observations for all days having remote sensing imagery. Model flux components were extracted from the image pixels in the vicinity of the flux towers. A simple analytical footprint model (Hsieh et al., 2000) applied to the measurement data, taken at ~ 2 m above ground level, predicted

Table 4
Difference statistics between TSEB and SEBAL $H$ output (TSEB − SEBAL) grouped by land cover class

| SGP '97 | | SEBAL | TSEB | | | | | SEBAL | TSEB |
|---|---|---|---|---|---|---|---|---|---|
| | | <$H$> | <$H$> | <$\Delta H$> | MAD | MAPD | RMSD | $z_{0m}$ | $z_{0m}$ |
| Landcover | $n$ | (W/m$^2$) | (W/m$^2$) | (W/m$^2$) | (W/m$^2$) | (%) | (W/m$^2$) | (m) | (m) |
| Bare soil | 45073 | 89 | 222 | 133 | 133 | 150 | 144 | 0.035 | 0.0060 |
| Pasture | 125602 | 91 | 119 | 27 | 27 | 30 | 38 | 0.210 | 0.0630 |
| Riparian | 14519 | 51 | 106 | 56 | 63 | 125 | 92 | 0.320 | 0.3750 |
| Water | 994 | 15 | 2 | −12 | 14 | 98 | 24 | 0.006 | 0.0004 |
| Monsoon '90 | | SEBAL | TSEB | | | | | SEBAL | TSEB |
| | | <$H$> | <$H$> | <$\Delta H$> | MAD | MAPD | RMSD | $z_{0m}$ | $z_{0m}$ |
| Landcover | $n$ | (W/m$^2$) | (W/m$^2$) | (W/m$^2$) | (W/m$^2$) | (%) | (W/m$^2$) | (m) | (m) |
| Bare soil | 4241 | 126 | 188 | 63 | 64 | 51 | 66 | 0.014 | 0.005 |
| Grassland | 43759 | 112 | 138 | 26 | 31 | 28 | 36 | 0.029 | 0.010 |
| Riparian | 3079 | 140 | 161 | 23 | 36 | 26 | 48 | 0.054 | 0.100 |
| Shrubland | 52201 | 129 | 169 | 41 | 42 | 33 | 47 | 0.019 | 0.050 |

Also listed are the average surface roughness values defined by each model for each class.

a maximum contribution within ~50 m of the tower. Therefore, pixels within, an area of ~60×60 m upwind of the flux tower site were averaged to represent the source area contributing to the flux observations. The performance of the models was evaluated using difference statistics suggested by Willmott (1982), listed in Table 2.

### 5.2. Model validation in comparison with flux tower observations

Comparisons between modeled and observed fluxes for Monsoon 90 and SGP '97 are shown in Fig. 2 and tabulated in Table 3. Similar levels of agreement were obtained for both experiments, and therefore they are not differentiated here.

Net radiation estimates from both models do not differ significantly (i.e., within ~ 50 W $m^{-2}$) with the observations, although SEBAL tends to underestimate this component. Soil heat fluxes for both schemes are also in reasonable agreement with ground observations.

With regard to the turbulent fluxes, *H* and LE, both models performed reasonably well. Sensible heat flux estimates from TSEB yielded an average Root Mean Square Difference (RMSD) of approximately 35 W $m^{-2}$ with respect to observations for both studies, while the average RMSD for *H* from SEBAL was nearly 50 W $m^{-2}$. RMSD values were higher for LE (60 and 70 W $m^{-2}$ for TSEB and SEBAL, respectively), but still considered in reasonable agreement with the tower measurements, which have intrinsic uncertainties on the order of 50 W $m^{-2}$ (Twine et al., 2000).

The effects of end-member selection for the 5 scenarios described in Section 4 are demonstrated in Fig. 3, showing changes in *H* of up to 50% for DOY 183 at SGP '97 for both schemes, depending on choice of end-member value. Again, the TSEB is most sensitive to changes in the upper limit of the NDVI scaling (scenario 4), while SEBAL shows similar sensitivity to the selection of hot and cold end-members at each of the tower sites. The site where SEBAL gives the largest errors in *H* (~ 100 W $m^{-2}$) was over dry, bare soil with high sensible heating rates. The TSEB is not sensitive to end-member selection for a bare soil site (see Fig. 3).

## 6. Model intercomparison

### 6.1. Intercomparison strategy

Flux towers are often placed in areas with relatively large (several hundred meters) homogenous fetch in order to facilitate

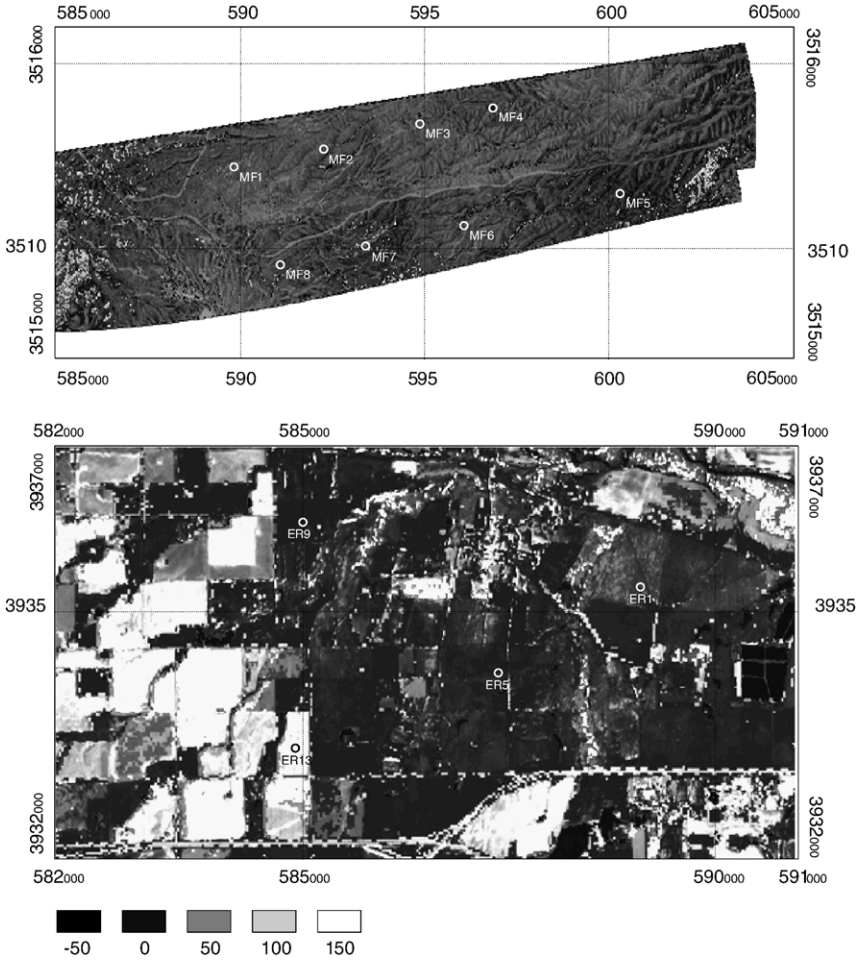


Fig. 4. Differences between SEBAL and TSEB modeled sensible heat flux (W/$m^2$) for Monsoon'90 DOY 221 (upper image) and SGP '97 DOY 183 (lower image). Differences are calculated by subtracting the SEBAL output from the TSEB output (TSEB-SEBAL). Approximate locations of the flux towers are also indicated.

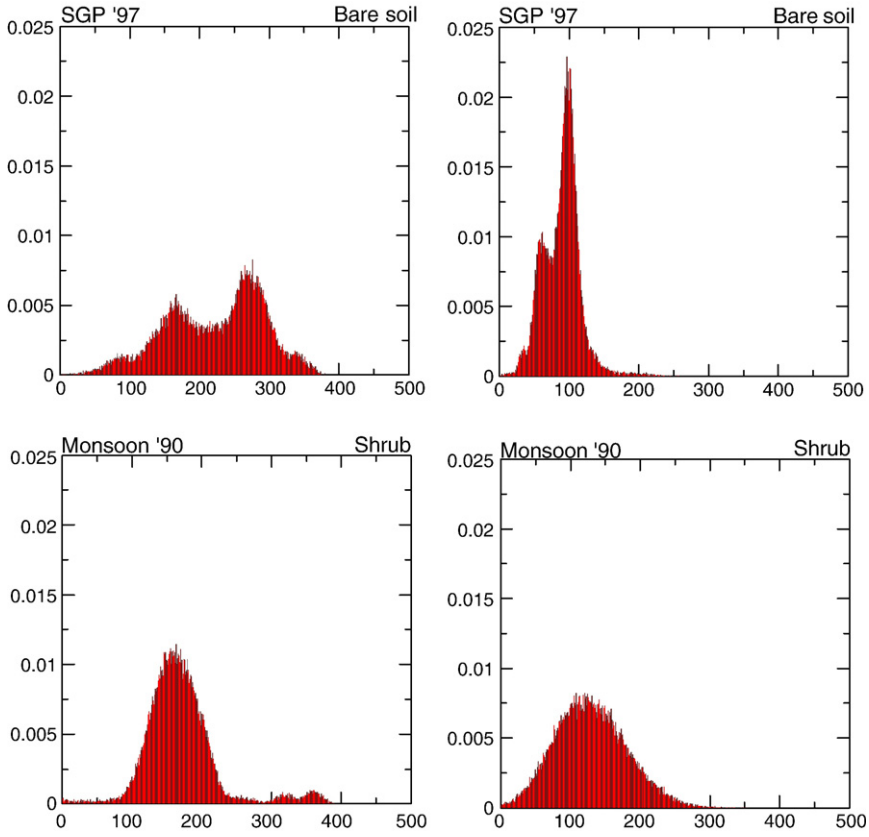


Fig. 5. Comparison between TSEB (the two left histograms) and SEBAL (the two right histograms) estimates of the spatial distribution of sensible heat flux for bare soil (SGP ’97 site) and shrub land (Monsoon ’90 site) cover types.

interpretation of the observations (Schuepp et al., 1990), and these sites will not typically be representative of the extreme or unique conditions that are of special interest in environmental monitoring (Moran, 2004). Good agreement with a handful of flux tower observations does not guarantee that the models compute consistent and/or reliable fluxes across a landscape. Therefore, a closer look was taken at spatial differences in flux fields generated by SEBAL and TSEB over the full modeling domains at SGP ’97 and Monsoon ’90.

To facilitate this, we focus here on 1 day from each field campaign, chosen to maximize the spatial variability in soil moisture conditions and evaporative fluxes over the modeling domains. This also facilitates the application of SEBAL since it requires that a full range in hydrological conditions be present within the scene. For Monsoon ’90, DOY 221 had the largest range in moisture and flux conditions (Schmugge et al., 1998), while for SGP ’97 the DOY 183 image was collected 4 days after a rainfall event and showed marked contrasts in surface temperature and fluxes (Norman et al., 2003).

Intercomparisons were performed for three sets of model runs. Case A uses local meteorological forcing and observations, applying the original TSEB and SEBAL schemes defining the various model input variables (as in the validation study in Section 5). Case B is identical to Case A, except that the SEBAL model is run using the more realistic values of momentum roughness used in TSEB for Case A, based on local field measurements and land cover information (see

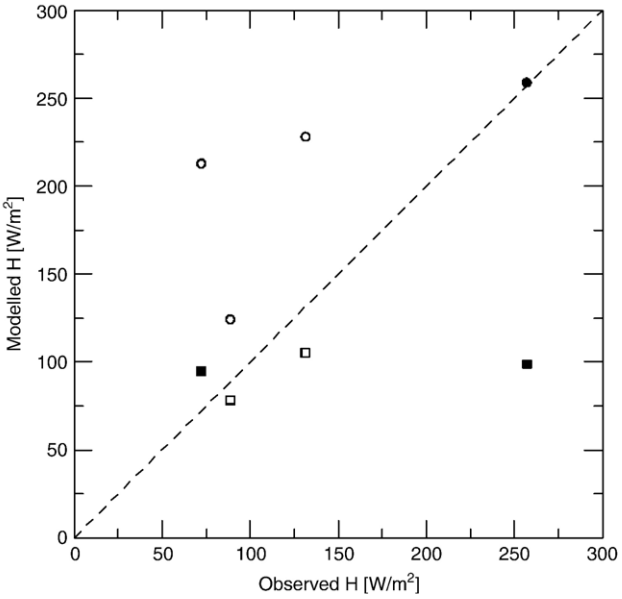


Fig. 6. SEBAL sensible heat output for DOY 183 in SGP ’97 versus $H$ observations under case A (squares) and modifying hot pixel end-member values (circles) of maximum surface temperature, $T_{\text{R-max}}$,, surface roughness, $z_{0m}$, and available energy, $R_N - G$, (see text). Open symbols represent the grassland/pasture sites (ER01, ER05 and ER09) and closed symbols are for the bare soil site (ER13).

Table 4); hence the TSEB run is the same as for Case A. In case C, the models are forced with remote meteorological data, and other model inputs for both models are set to nominal values (no local information used). For case C, both models use only first order estimates of standard meteorological inputs (radiation, air temperature, wind speed and relative humidity) from remote meteorological stations for these two regions (i.e. 75 and 120 km from the SGP '97 and Monsoon '90 study sites, respectively; see Norman et al., 2000). The TSEB model was run using nominal values for the canopy height and other vegetation variables assigned to each land cover class, while SEBAL used the NDVI formulation (Eq. (5)) for defining momentum roughness across the scene.

### 6.2. Case A: local inputs

Maps showing discrepancies in the $H$ fields generated by the two models for Monsoon'90 DOY 221 and SGP '97 DOY 183 using local inputs (Case A) are shown in Fig. 4. Despite the acceptable agreement with flux measurements at the tower sites, predictions of sensible heating from the two schemes differ by more than 100 W $m^{-2}$ in some areas (see Table 4).

It is clear, particularly for the SGP '97 scene, that the differences occur in contiguous patches related to land cover. Statistics comparing estimates of H from both models, stratified by land cover class, are provided in Table 4.

The largest discrepancies exist over bare soil, where SEBAL estimates of H are significantly lower than those from TSEB. The TSEB estimates are in better agreement with observations made over bare soil during SGP '97 (Fig. 3).

Histograms of $H$ predicted by the two modeling schemes for the Monsoon '90 shrub class and the SGP '97 bare soil class show very different distributions and mean values (Fig. 5). Similar differences, but to a lesser extent, are observed for all other land cover types for both landscapes, where the TSEB consistently predicts larger values of H on average than does SEBAL.

The difference in $H$ distribution is particularly notable for the bare soil class, where one- and two-source models should theoretically give similar output. The distributions for the shrub class in Monsoon '90 are also quite different, with values from TSEB being more centrally peaked. Flux distributions from the two models were most similar for the grassland and pasture cover class, which tended to have a more uniform canopy cover.

Difficulty in estimating $H$ over sparsely vegetated surfaces is a well-known phenomenon when dealing with one-source models, and corrections are usually made by adjusting the roughness length for heat or the $kB^{-1}$ parameter (e.g., Stewart et al., 1994; Verhoef et al., 1997) or by including empirical "extra resistance" factors, parameterized to match observed fluxes. However, it is not clear how to generalize these empirical adjustments for different land cover types and cover conditions under a one-source scheme. The two-source approach provides a more physical framework for estimating spatial variability in aerodynamic surface resistance by directly considering the effects of varying vegetation cover amount on the coupling between the soil and atmosphere through the soil resistance, $r_s$, in Eq. (8) (Kustas & Norman, 1999).

To isolate differences in model parameterizations of $H$ from differences in specification of $R_N$ and $G$, both models were also run using identical fields of $R_N$ and $G$ (generated by TSEB). While this resulted in slight improvements in agreement between the modeled $H$ fields, they still showed major discrepancies associated with land cover type. The MAD between modeled $H$ for the Monsoon site was approximately 60, 25, 20 and 35 W $m^{-2}$ for bare soil, grassland, riparian and shrubland areas, respectively. For the SGP site, the MAD in $H$ was around 120, 30, 80 and 20 W $m^{-2}$ for bare soil, pasture, riparian and water bodies, respectively. RMSD values for the two sites were similar to those in Table 4 when both models

Table 5
Average $H$ output and differences between TSEB and SEBAL (TSEB − SEBAL) for the different cases, grouped by land cover class

| SGP '97 | Case A (same results listed in Table 4) | | | Case B | | | Case C | | |
|---|---|---|---|---|---|---|---|---|---|
| | SEBAL | TSEB | | SEBAL | TSEB | | SEBAL | TSEB | |
| Landcover | <$H$> (W/m$^2$) | <$H$> (W/m$^2$) | <$\Delta H$> (W/m$^2$) | <$H$> (W/m$^2$) | <$H$> (W/m$^2$) | <$\Delta H$> (W/m$^2$) | <$H$> (W/m$^2$) | <$H$> (W/m$^2$) | <$\Delta H$> (W/m$^2$) |
| Bare soil | 89 | 222 | 133 | 49 | 222 | 173 | 94 | 255 | 161 |
| Pasture | 91 | 119 | 27 | 60 | 119 | 59 | 122 | 217 | 95 |
| Riparian | 51 | 106 | 56 | 88 | 106 | 18 | 84 | 271 | 187 |
| Water | 15 | 2 | −12 | 26 | 2 | −24 | 39 | −11 | −50 |
| **Monsoon '90** | **Case A (same results listed in Table 4)** | | | **Case B** | | | **Case C** | | |
| | SEBAL | TSEB | | SEBAL | TSEB | | SEBAL | TSEB | |
| Landcover | <$H$> (W/m$^2$) | <$H$> (W/m$^2$) | <$\Delta H$> (W/m$^2$) | <$H$> (W/m$^2$) | <$H$> (W/m$^2$) | <$\Delta H$> (W/m$^2$) | <$H$> (W/m$^2$) | <$H$> (W/m$^2$) | <$\Delta H$> (W/m$^2$) |
| Bare soil | 126 | 188 | 63 | 78 | 188 | 110 | 121 | 180 | 59 |
| Grassland | 112 | 138 | 26 | 67 | 138 | 71 | 110 | 130 | 20 |
| Riparian | 140 | 161 | 23 | 154 | 161 | 7 | 207 | 174 | −33 |
| Shrubland | 129 | 169 | 41 | 150 | 169 | 19 | 128 | 151 | 23 |

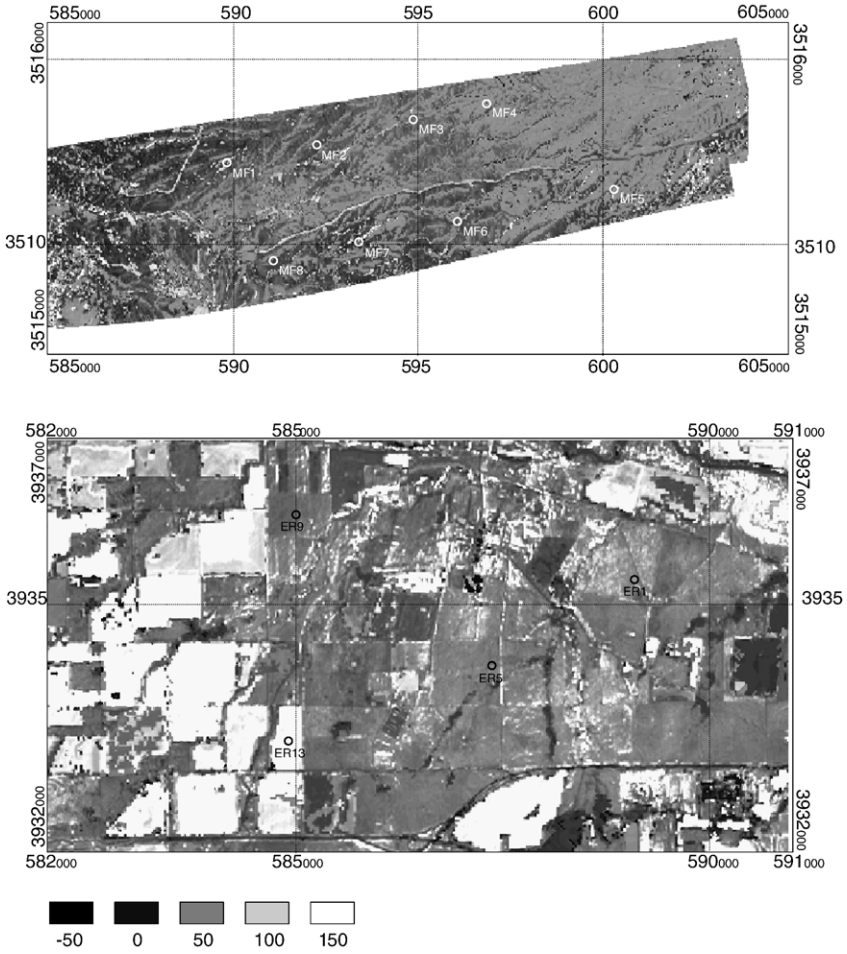


Fig. 7. Differences between SEBAL and TSEB modeled sensible heat flux (W $m^{-2}$) under case B (see text) for Monsoon '90 DOY 221 (upper image) and SGP '97 DOY 183 (lower image). Differences are calculated by subtracting the SEBAL output from the TSEB output (TSEB-SEBAL). Approximate locations of the flux towers are also indicated.

used the same $R_N$ and $G$. Therefore, differences in available energy computations between the models were not a major cause of the discrepancies in $H$ and LE.

Attempts to adjust the end-members in surface temperature to achieve improvement in agreement with TSEB estimates and tower observations of $H$ over bare soil surfaces caused degradation in agreement over vegetated areas. This is demonstrated in Fig. 6, where $T_{R\text{-}max}$ was chosen such that the SEBAL estimate of H at the bare soil site in SGP '97 reproduced the observed flux on DOY 183.

Using $T_{R\text{-}max}=327$ K, and available energy and $z_{0m}$ appropriate for bare soil as the hot pixel end-member, SEBAL now gives excellent agreement with $H$ observed over the bare soil site, but ~100 W $m^{-2}$ differences (overestimates) with observed $H$ for two of three grassland pasture sites (Fig. 6).

This behavior is due in part to the sensitivity of SEBAL to selection of dry end-members, as demonstrated in Fig. 3. Obtaining the coefficients for Eq. (4) involves flux inversion at the dry end, as $H$ at the wet end is assumed to be 0. The value of $\delta T_{asur}$ retrieved at the dry end will depend on the magnitude of $r_{ah}$ estimated for that pixel. Therefore, the fundamental linear relationship between $T_R$ and $\delta T_{asur}$ used in SEBAL (Eq. (6)) is driven to a large extent by the roughness conditions assumed at the selected dry end-member pixels. Residual errors in the specification of $z_{0h}$ and $z_{0m}$ at this pixel are absorbed into the retrieved $\delta T_{asur}$ endpoint, and therefore the regression is tuned to the specific characteristics of that pixel. The resulting regression will therefore give better agreement for areas with comparable roughness characteristics ($z_{0h}$ and $z_{0m}$) because the errors will be similar in these areas. However, it may yield poor

Table 6
Difference statistics for $H$ output (W $m^{-2}$) with respect to observations for different cases A, B, and C described in the text

| Variable | Case A | | Case B | | Case C | |
|---|---|---|---|---|---|---|
| | SEBAL | TSEB | SEBAL | TSEB | SEBAL | TSEB |
| $N$ | 12 | 12 | 12 | 12 | 12 | 12 |
| $<O>$ | 146 | 146 | 146 | 146 | 146 | 146 |
| $<P>$ | 115 | 161 | 94 | 161 | 120 | 169 |
| So | 47 | 47 | 47 | 47 | 47 | 47 |
| Sp | 30 | 53 | 44 | 53 | 28 | 63 |
| MAD | 41 | 22 | 59 | 22 | 47 | 38 |
| MAPD | 28 | 15 | 40 | 15 | 32 | 26 |
| RMSD | 56 | 30 | 74 | 30 | 59 | 48 |

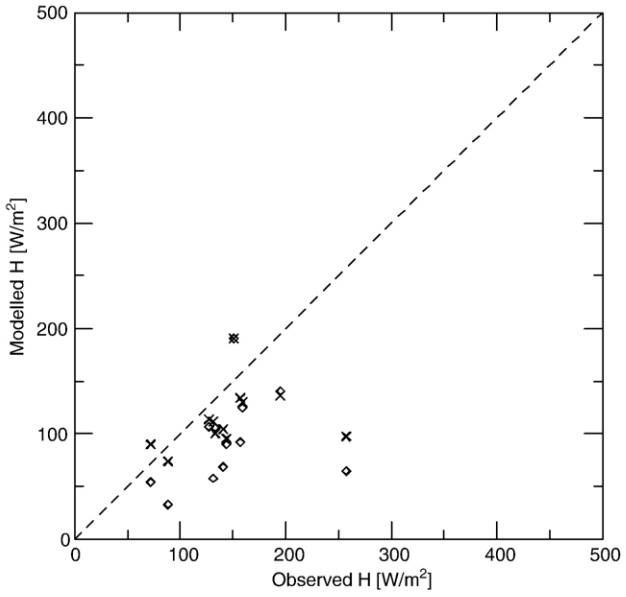


Fig. 8. SEBAL estimated versus observed $H$ values (W m$^{-2}$) for Case A (using momentum roughness values from Eq. (5); $X$ symbols) and Case B (using realistic roughness values; diamond symbols).

results for areas having roughness characteristics very different from those of the dry end-member. This suggests another type of normalization procedure that incorporates land cover type would be preferable, as suggested by Su (2002).

### 6.3. Case B: realistic roughness estimates

In Case A, there is clearly a problem with the estimation of surface roughness length for momentum, $z_{0m}$, via Eq. (5) in the original version of SEBAL (Bastiaanssen et al., 1998a), where roughness is linked only to NDVI. For the Monsoon'90 dataset, Eq. (5) yields lower average roughness estimates for the shrubland than for the grassland areas (see Table 4), contradicting roughness observations made in the field (Menenti & Ritchie, 1994). Re-calibration of Eq. (5), or attempts to use other indices, corrected for bare soil influences (Bastiaanssen, 2000), do not improve roughness estimates since the exponential behavior of the relation ensures either a monotonic increase or decrease with increasing NDVI. As such, this equation will not be able to capture typical roughness distributions for bare soil, grassland and shrub landcover, as it does not consider a major factor affecting roughness, namely the vegetation height (e.g., in forested areas). Tasumi et al. (2000), proposed a more physically-based formulation, using a multi-linear approach and applying separate sets of coefficients in Eq. (5) for separate land cover classes. Other remote sensing-based approaches should also be explored (Hasager & Jensen, 1999; Jasinski & Crago, 1999).

When the more realistic surface roughness values from TSEB are used in both models, model discrepancies are reduced for the riparian classes and for the shrubland class in Monsoon '90; however, differences increase significantly for all other classes (compare Tables 4 and 5, and Figs. 4 and 7).

In particular, model agreement deteriorates over bare soil and agreement between SEBAL and observed fluxes also deteriorates when the more realistic values of roughness are used (Table 6). The RMSD between measured and SEBAL model H estimates for both experiments combined increases from ~55 W m$^{-2}$ for Case A to ~75 W m$^{-2}$ for Case B (Table 6 and Fig. 8).

In comparison, the TSEB yields a RMSD of 30 W m$^{-2}$ using the same roughness fields (Table 6 and Fig. 9a.).

The fact that SEBAL does not work as well with physically realistic roughness data raises questions about the robustness of the algorithm over complex landscapes such as in SGP '97 and Monsoon '90, where roughness and moisture conditions vary widely across the modeling scene, resulting in potentially significant deviations from the linear relationship between $T_R$ and $\delta T_{asur}$ assumed in Eq. (6) (Norman et al., 2006).

### 6.4. Case C: remote inputs

Comparisons between observed and model $H$ results for case C are illustrated in Fig. 9b and suggest that both models perform similarly at the Monsoon '90 and SGP '97 tower sites using no local ancillary data. The RMSD values between modeled and

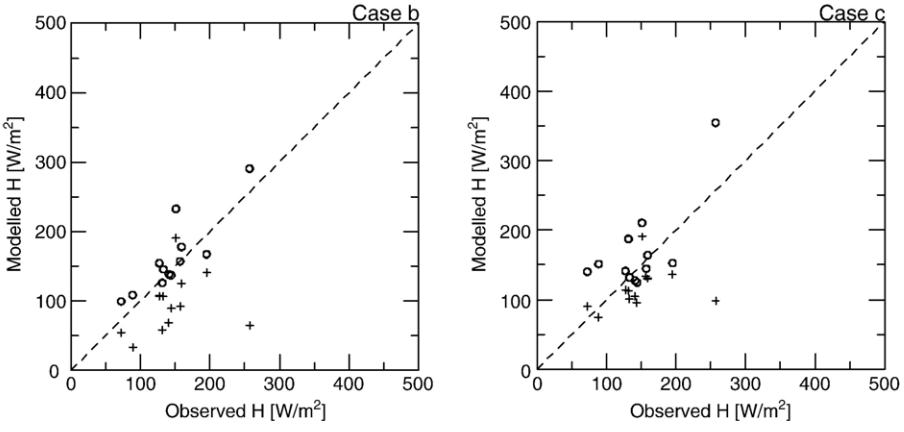


Fig. 9. Modeled versus observed sensible heat fluxes (W m$^{-2}$) for Monsoon '90 (DOY 221) and SGP '97(DOY 183) for both schemes under the different scenarios (case B and C) described in the text. The cross symbols represent SEBAL and the circles represent TSEB output.

measured fluxes are around 50 and 60 W $m^{-2}$ for the TSEB model and SEBAL, respectively (Table 6). While this represents only a slight increase in RMSD for SEBAL over case A, the increase in TSEB model discrepancies with observations are more significant (i.e., from 30 W $m^{-2}$ for Case A), primarily due to model-observation differences for the SGP site. One of the strengths of SEBAL is that has been designed specifically to use only nominal estimates of meteorological conditions, available globally with adequate accuracy from regional weather stations or simulations. When employed within the coupled land surface-ABL modeling scheme (Anderson et al., 1997, 2005; Kustas et al., 2001), however, the TSEB functions similarly with both local and remote meteorological inputs.

## 7. Summary and conclusions

An intercomparison of output from two remote sensing-based surface energy balance models is conducted over a range of environmental conditions. SEBAL is a single-source model requiring minimal ancillary data, but requiring subjective specifications of representative hot/dry and wet/cool end-member pixels within the scene to define model parameters/variables. The second model examined, TSEB, is a two-source (soil+vegetation) approach, which can be applied to any landscape condition but requires ancillary inputs, most importantly meteorological data and vegetation cover, for computing reliable fluxes. Validation at specific sites using tower flux observations showed that, in general, results from both models were acceptable, although SEBAL had difficulties estimating appropriate fluxes near the hydrologic extremes, particularly the relatively dry areas.

A sensitivity analysis of TSEB and SEBAL to errors in principle inputs revealed that uncertainty in remotely sensed surface temperature had a significant effect on heat flux estimation from both models, with somewhat higher sensitivity for TSEB. For SEBAL, the choice of end-members in surface temperature defining the dry and wet pixels for the image had a significant effect on flux output. The TSEB model also had sensitivity to uncertainties in fractional vegetation cover and/or leaf area index. This sensitivity was greater at the high cover condition where small variations in cover have a significant effect on soil and canopy temperature estimation.

While both models showed similar agreement with tower observations collected during two field experiments, spatial agreement in sensible heat flux between the two models was generally poor, depending on land cover type. The largest discrepancies between TSEB and SEBAL occurred over bare soil and dry/sparsely vegetated areas, where TSEB was in better agreement with observations. Attempts to tune SEBAL by adjusting temperature end-members or momentum roughness ($z_{0m}$) inputs improved model agreement for some land classes while exacerbating discrepancies in other land use groups.

An empirical expression for estimating $z_{0m}$ based on remotely sensed NDVI (Eq. (5)), used in the original form of SEBAL (Bastiaanssen et al., 1998a), generated unrealistic roughness values over the semi-arid field site of the Monsoon '90 experiment, which was characterized by grassland with high NDVI and low roughness, and sparse shrubland with low NDVI and relatively high roughness. Use of more realistic roughness fields in SEBAL generally degraded model agreement with observed fluxes. This suggests that the internal calibration procedures in SEBAL, particularly the assumption of linearity between surface temperature and the aerodynamic temperature gradient used in defining the sensible heat fluxes, do not appear to be generally valid for this kind of strongly heterogeneous landscape. The simulation studies of Norman et al. (2006) suggest that several linear relationships between $T_R$ and $\delta T_{asur}$, with significantly different slopes, can in fact exist within a given landscape depending on the variability in roughness and moisture stress conditions present within the constituent land cover classes.

The selection of the end-member pixels, particularly at the dry end, can have a significant impact on the heat flux distribution from SEBAL (Fig. 6). The results presented here suggest that errors in roughness specification at the dry pixel propagate into the regression equation used to retrieve $\delta T_{asur}$ (Eq. (6)) and can corrupt flux estimates in areas with moisture and roughness characteristics very different from those in the dry pixel. In the case of DOY 183 during SGP '97, appropriate end-member selections could be identified yielding good sensible heating rates over hot, bare soil or over unstressed pasture, but no single selection satisfied both conditions.

A comparison between sensible heat fields generated by the TSEB and SEBAL models using remote meteorological data, with other inputs for both models set to nominal values (no local information used), indicated similar agreement with flux tower observations. In this case, with minimal ancillary information the reliability of SEBAL and the TSEB model flux estimates was comparable. For regional applications, air temperature boundary conditions can be supplied to the TSEB through a coupled ABL modeling scheme, further reducing sensitivity to errors in ancillary data fields (Anderson et al., 2007).

To gain greater insight, efforts are underway (Norman et al., 2006) to evaluate both the TSEB and SEBAL schemes under a much wider set of conditions generated from a complex soil–plant–atmosphere model Cupid (Norman & Campbell, 1983). Cupid simulates the transport of energy, mass and momentum between plants and their soil and atmospheric environments and computes the fluxes as well as aerodynamic and most importantly radiometric temperature. Consequently, Cupid provides a unique opportunity to assess the performance of remote sensing-based models under a wider range of conditions than observed experimentally (Kustas et al., 2006a,b, 2004). These types of investigations should ultimately lead to improved parameterizations and potentially to the development of a hybrid model incorporating the strengths of both SEBAL and the TSEB modeling schemes, as suggested by Norman et al. (2006), having greater operational utility under a wider range of landscape and environmental conditions.

## Acknowledgements

The financial support and cooperation of the staff at the Hydrology and Remote Sensing Laboratory, USDA-ARS,

Beltsville, Maryland were critical to the successful execution of this study.

## References


Anderson, M. C., Kustas, W. P., & Norman, J. M. (2003). Upscaling and downscaling — A regional view of the soil–plant–atmosphere continuum. *Agronomy Journal*, *95*, 1408−1423.

Anderson, M. C., Kustas, W. P., & Norman, J. M. (2007). Upscaling tower and aircraft fluxes from local to continental scales using thermal remote sensing. *Agronomy Journal*, *99*, 240−254.

Anderson, M. C., Norman, J. M., Diak, G. R., Kustas, W. P., & Mecikalski, J. R. (1997). A two-source time-integrated model for estimating surface fluxes using thermal infrared remote sensing. *Remote Sensing of Environment*, *60*, 195−216.

Anderson, M. C., Norman, J. M., Kustas, W. P., Li, F., Prueger, J. H., & Mecikalski, J. R. (2005). Effects of vegetation clumping on two-source model estimates of surface energy fluxes from an agricultural landscape during SMACEX. *Journal of Hydrometeorology*, *6*, 892−909.

Anderson, M. C., Norman, J. N., Mecikalski, J. R., Torn, R. D., Kustas, W. P., & Basara, J. B. (2004). A multi-scale Remote Sensing Model for disaggregating regional fluxes to micrometeorological scales. *Journal of Hydrometeorology*, *5*, 343−363.

Avissar, R., & Pielke, R. A. (1989). A parameterization of heterogeneous land surfaces for atmospheric numerical models and its impact on regional meteorology. *Monthly Weather Review*, *117*, 2113−2136.

Bastiaanssen, W. G. M. (1995). Regionalization of surface flux densities and moisture indicators in composite terrain — A remote sensing approach under clear skies in Mediterranean climates. PhD thesis — Wageningen Agricultural University, The Netherlands ISBN 90-5485-465-0, pp 273.

Bastiaanssen, W. G. M. (2000). SEBAL-based sensible and latent heat fluxes in the irrigated Gediz Basin, Turkey. *Journal of Hydrology*, *229*, 87−100.

Bastiaanssen, W. G. M., Ahmad, M. -u. -D., & Chemin, Y. (2002). Satellite surveillance of evaporative depletion across the Indus Basin. *Water Resources Research*, *38*(12). doi:10.1029/2001WR000386.

Bastiaanssen, W. G. M., Menenti, M., Feddes, R. A., & Holtslag, A. A. M. (1998). A remote sensing surface energy balance algorithm for land (SEBAL): 1. Formulation. *Journal of Hydrology*, *212–213*, 198−212.

Bastiaanssen, W. G. M., Noordman, E. J. M., Pelgrum, H., Davids, G., Thoreson, B. P., & Allen, R. G. (2005). SEBAL model with remotely sensed data to improve water-resources management under actual field conditions. *Journal of Irrigation and Drainage Engineering*, *131*, 85−93.

Bastiaanssen, W. G. M., Pelgrum, H., Wang, J., Ma, Y., Moreno, J. F., Roerink, G. J., et al. (1998). A remote sensing surface energy balance algorithm for land (SEBAL): 2. Validation. *Journal of Hydrology*, *212–213*, 213−229.

Brutsaert, W. (1982). *Evaporation into the atmosphere* (pp. 299). Dordrecht: Reidel.

Campbell, G. S., & Norman, J. M. (1998). *An introduction to environmental biophysics.* New York: Springer. ISBN 0-387-94937-2. 286 pp.

Choudhury, B. J. (1987). Relationships between vegetation indices, radiation absorption, and net photosynthesis evaluated by a sensitivity analysis. *Remote Sensing of Environment*, *22*, 209−233.

Choudhury, B. J., Ahmed, N. U., Idso, S. B., Reginato, R. J., & Daughtry, C. S. T. (1994). Relations between evaporation coefficients and vegetation indices studied by model simulations. *Remote Sensing of Environment*, *50*, 1−17.

Crow, W. T., & Kustas, W. P. (2005). Utility of assimilating surface radiometric temperature observations for evaporative fraction and heat transfer coefficient retrieval. *Bound-Layer Meteorology*, *115*, 105−130.

Diak, G. R., Mecikalski, J. R., Anderson, M. C., Norman, J. M., Kustas, W. P., Torn, R. D., et al. (2004). Estimating land-surface energy budgets from space: Review and current efforts at the University of Wisconsin–Madison and USDA-ARS. *Bulletin of the American Meteorological Society*, *85*(1), 65−78.

French, A. N., Jacob, F., Anderson, M. C., Kustas, W. P., Timmermans, W. J., Gieske, A., et al. (2005). Surface energy fluxes with the Advanced Spaceborne Thermal Emission and Reflection radiometer (ASTER) at the Iowa 2000 SMACEX site (USA). *Remote Sensing of Environment*, *99*, 55−65 (Corrigendum 99, 471).

French, A. N., Kustas, T. J., & Kustas, W. P. (2000). Estimating surface fluxes over the SGP site with remotely sensed data. *Physics and Chemistry of the Earth. Part B: Hydrology, Oceans and Atmosphere*, *25*, 167−172.

French, A. N., Norman, J. M., & Anderson, M. C. (2003). A simple and fast atmospheric correction for spaceborne remote sensing of surface temperature. *Remote Sensing of Environment*, *87*, 326−333.

French, A. N., Schmugge, T. J., Kustas, W. P., Brubaker, K. L., & Prueger, J. (2003). Surface energy fluxes over El Reno, Oklahoma, using high-resolution remotely sensed data. *Water Resources Research*, *39*(6), 1164. doi:10.1029/2002WR1734.

Garratt, J., & Hicks, B. (1973). Momentum, heat and water vapour transfer to and from natural and artificial surfaces. *Quarterly Journal of the Royal Meteorological Society*, *99*, 680−687.

Gieske, A. (2003). The iterative flux-profile method for remote sensing applications. *International Journal of Remote Sensing*, *24*, 3291−3310.

Hasager, C. B., & Jensen, N. O. (1999). Surface-flux aggregation in heterogeneous terrain. *Quarterly Journal of the Royal Meteorological Society*, *125*, 2075−2102.

Hsieh, C. -I., Katul, G., & Chi, T. -W. (2000). An approximate analytical model for footprint estimation of scalar fluxes in thermally stratified atmospheric flows. *Advances in Water Resources*, *23*, 765−772.

Humes, K. S., Kustas, W. P., & Goodrich, D. C. (1997). Spatially distributed sensible heat flux over a semiarid watershed. Part 1: Use of radiometric surface temperature and a spatially uniform resistance. *Journal of Applied Meteorology*, *36*, 281−292.

Huntingford, C., Verhoef, A., & Stewart, H. (2000). Dual versus single source models for estimating surface temperature of African savannah. *Hydrology and Earth System Sciences*, *4*, 185−191.

Jackson, T. J., Vine, D. M. L., Hsu, A. Y., Oldak, A., Starks, P. J., Swift, C. T., et al. (1999). Soil moisture mapping at regional scales using microwave radiometry: The Southern Great Plains hydrology experiment. *IEEE Transactions on Geoscience and Remote Sensing*, *37*, 2136−2151.

Jacob, F., Olioso, A., Gu, X. F., Su, Z., & Seguin, B. (2002). Mapping surface fluxes using airborne visible, near infrared, thermal infrared remote sensing data and a spatialized surface energy balance model. *Agronomie*, *22*, 669−680.

Jasinski, M. F., & Crago, R. D. (1999). Estimation of vegetation aerodynamic roughness of natural regions using frontal area density determined from satellite imagery. *Agricultural and Forest Meteorology*, *94*, 65−77.

Kustas, W. P. (1990). Estimates of evapotranspiration within a one- and two-layer model of heat transfer over partial vegetation cover. *Journal of Applied Meteorology*, *29*, 704−715.

Kustas, W. P., Anderson, M. C., French, A. N., & Vickers, D. (2006). Using a remote sensing field experiment to investigate flux-footprint relations and flux sampling distributions for tower and aircraft-based observations. *Advances in Water Resources*, *29*, 355−368.

Kustas, W. P., Anderson, M. C., Norman, J. M., & Li, F. (2006). Utility of radiometric–aerodynamic temperature relations for heat flux estimation. *Boundary-Layer Meteorology.* doi:10.1007/s10546-006-9093.

Kustas, W. P., Bindlish, R., French, A. N., & Schmugge, T. J. (2003). Comparison of energy balance modeling schemes using microwave-derived soil moisture and radiometric surface temperature. *Water Resources Research*, *39*, 1029. doi:10.1029/2002WR001361.

Kustas, W. P., Diak, G. R., & Norman, J. M. (2001). Time difference methods for monitoring regional scale heat fluxes with remote sensing. In V. Lakshmi, J. Albertson, & J. Schaake (Eds.), *Observations and modeling of the land surface hydrological processesAmerican Geophysical Union Water Science and Application Series*, *Vol. 3*. (pp. 15−29).

Kustas, W. P., Humes, K. S., Norman, J. M., & Moran, M. S. (1996). Single- and dual-source modeling of surface energy fluxes with radiometric surface temperature. *Journal of Applied Meteorology*, *35*, 110−121.

Kustas, W. P., Moran, M. S., Humes, K. S., Stannard, D. I., Pinter, J., Jr., Hipps, L. E., et al. (1994). Surface energy balance estimates at local and regional scales using optical remote sensing from an aircraft platform and atmospheric data collected over semiarid rangelands. *Water Resources Research*, *30*, 1241−1259.

Kustas, W. P., & Norman, J. M. (1996). Use of remote sensing for evapotranspiration monitoring over land surfaces. *Hydrological Sciences*, *41*, 495−516.

Kustas, W. P., & Norman, J. M. (1999). Evaluation of soil and vegetation heat flux predictions using a simple two-source model with radiometric temperatures for partial canopy cover. *Agricultural and Forest Meteorology*, *94*, 13−29.

Kustas, W. P., Norman, J. M., Schmugge, T. J., & Anderson, M. C. (2004). Mapping surface energy fluxes with radiometric temperature. In D. A. Quattrochi & J. C. Luvall (Eds.), *Thermal remote sensing in land surface processes* (pp. 205−253). Boca Raton. Florida: CRC Press.

Lhomme, J. P., Monteney, B., & Amadou, M. (1994). Estimating sensible heat flux from radiometric temperature over sparse millet. *Agricultural Water Management*, *68*, 77−91.

Li, F., Kustas, W. P., Prueger, J. H., Neale, C. M. U., & Jackson, T. J. (2005). Utility of remote sensing based two-source energy balance model under low- and high-vegetation cover conditions. *Journal of Hydrometeorology*, *6*, 878−891.

Matsushima, D. (2005). Relations between aerodynamic parameters of heat transfer and thermal-infrared thermometry in the bulk surface formulation. *Journal of the Meteorological Society of Japan*, *83*, 373−389.

Mecikalski, J. R., Diak, G. R., Anderson, M. C., & Norman, J. M. (1999). Estimating fluxes on continental scales using remotely sensed data in an atmospheric-land exchange model. *Journal of Applied Meteorology*, *38*, 1352−1369.

Menenti, M., & Ritchie, J. C. (1994). Estimation of effective aerodynamic roughness of Walnut Gulch watershed with laser altimeter measurements. *Water Resources Research*, *30*, 1329−1337.

Merlin, O., & Chehbouni, A. (2004). Different approaches in estimating heat flux using dual angle observations of radiative surface temperature. *International Journal of Remote Sensing*, *25*(1), 275−289.

Moran M. S. (2004). Thermal infrared measurements as an indicator of plant ecosystem health. In: *"Thermal Remote Sensing in Land Surface Processes"*, ed. D.A. Quattrochi, and J. Luvall, Taylor and Francis. CRC Press. Boca Raton, Florida, USA, pp. 257−282.

Nemani, R. R., & Running, S. W. (1989). Estimation of regional surface resistance to evapotranspiration from NDVI and thermal-IR AVHRR data. *Journal of Applied Meteorology*, *28*, 276−284.

Norman, J. M., Anderson, M. C., & Kustas, W. P. (2006). Are single-source, remote-sensing surface-flux models too simple? In G. D'Urso, M. A. Osann Jochum, & J. Moreno (Eds.), *Proceedings of the international conference on earth observation for vegetation monitoring and water management*, *Vol. 852*. (pp. 170−177). American Institute of Physics.

Norman, J. M., Anderson, M. C., Kustas, W. P., French, A. N., Mecikalski, J. R., Torn, R. D., et al. (2003). Remote sensing of surface energy fluxes at 101-m pixel resolutions. *Water Resources Research*, *39*(8), 1221. doi:10.1029/2002WR001775.

Norman, J. M., & Campbell, G. S. (1983). Application of a plant-environment model to problems in irrigation. In D. I. Hillel (Ed.), *Advances in irrigation*, *Vol. II*. (pp. 155−188). New York: Academic Press.

Norman, J. M., Kustas, W. P., & Humes, K. S. (1995). A two-source approach for estimating soil and vegetation energy fluxes in observations of directional radiometric surface temperature. *Agricultural and Forest Meteorology*, *77*, 263−293.

Norman, J. M., Kustas, W. P., Prueger, J. H., & Diak, G. R. (2000). Surface flux estimation using radiometric temperature: A dual-temperature-difference method to minimize measurement errors. *Water Resources Research*, *36*, 2263−2274.

Prihodko, L., & Goward, S. N. (1997). Estimation of air temperature from remotely sensed surface observations. *Remote Sensing of Environment*, *60*, 335−346.

Prince, S. D., Goetz, S. J., Dubayah, R. O., Czajkowski, K. P., & Thawley, M. (1998). Inference of surface and air temperature, atmospheric precipitable water and vapor pressure deficit using Advanced Very High-Resolution Radiometer satellite observations: Comparison with field observations. *Journal of Hydrology*, *212*, 230−249.

Ross, J. (1975). Radiative transfer in plant communities. In J. L. Monteith (Ed.), *Vegetation and the atmosphere* (pp. 13−55). London: Academic Press.

Schmugge, T. J., Kustas, W. P., & Humes, K. S. (1998). Monitoring land surface fluxes using ASTER observations. *IEEE Transactions on Geoscience and Remote Sensing*, *36*, 1421−1430.

Schuepp, P. H., Leclerc, M. Y., Macpherson, J. I., & Desjardins, R. L. (1990). Footprint prediction of scalar fluxes from analytical solutions of the diffusion equation. *Boundary-Layer Meteorology*, *50*, 355−373.

Shuttleworth, J. W., & Wallace, J. S. (1985). Evaporation from sparse crops — An energy combination theory. *Quarterly Journal of the Royal Meteorological Society*, *111*, 839−855.

Song, J., Wesely, M. L., LeMone, M. A., & Grossman, R. L. (2000). Estimating watershed evapotranspiration with PASS. Part II: Moisture budgets during drydown periods. *Journal of Hydrometeorology*, *1*, 462−473.

Stewart, J. B., Kustas, W. P., Humes, K. S., Nichols, W. D., Moran, M. S., & de Bruin, H. A. R. (1994). Sensible heat flux-radiometric surface temperature relationship for 8 semi-arid areas. *Journal of Applied Meteorology*, *33*, 1110−1117.

Su, Z. (2002). The Surface Energy Balance System (SEBS) for estimation of turbulent heat fluxes. *Hydrology and Earth System Sciences*, *6*, 85−99.

Su, Z., Pelgrum, H., & Menenti, M. (1999). Aggregation effects of surface heterogeneity in land surface processes. *Hydrology and Earth System Sciences*, *3*, 549−563.

Su, Z., Schmugge, T., Kustas, W. P., & Massman, W. J. (2001). An evaluation of two models for estimation of the roughness height for heat transfer between the land surface and the atmosphere. *Journal of Applied Meteorology*, *40*, 1933−1951.

Tasumi M., Allen, R. G., & Bastiaanssen, W. G. M. (2000). The theoretical basis of SEBAL. In A. Morse, M. Tasumi, R. G. Allen, & W. Kramber (Eds.), Application of the SEBAL methodology for estimating consumptive use of water and streamflow depletion in the Bear River basin of Idaho through remote sensing. Final report to the Raytheon Systems Company, Earth Observation System Data and Information System Project. Idaho Department of Water Resources and University of Idaho, 107 pp.

Troufleau, D., Lhomme, J. P., Monteny, B., & Vidal, A. (1997). Sensible heat flux and radiometric surface temperature over sparse Sahelian vegetation.I. An experimental analysis of the $kB^{-1}$ parameter. *Journal of Hydrology*, *188* (189), 815−838.

Twine, T. E., Kustas, W. P., Norman, J. M., Cook, D. R., Houser, P. R., Meyers, T. P., et al. (2000). Correcting eddy−covariance flux underestimates over a grassland. *Agricultural and Forest Meteorology*, *103*, 279−300.

Verhoef, A., McNaughton, K. G., & Jacobs, A. F. G. (1997). A parameterization of momentum roughness length and displacement height for a wide range of canopy densities. *Hydrology and Earth System Sciences*, *1*, 81−91.

Willmott, C. J. (1982). Some comments on the evaluation of model performance. *Bulletin of the American Meteorological Society*, *63*, 1309−1313.

Zhan, X., Kustas, W. P., & Humes, K. S. (1996). An intercomparison study on models of sensible heat flux over partial canopy surfaces with remotely sensed surface temperature. *Remote Sensing of Environment*, *58*, 242−256.